



Zwitterionic hybrid aerobeads of binary metal organic frameworks and cellulose nanofibers for removal anionic pollutants

Mohammad KarzarJeddi^{a,b}, Ossi Laitinen^a, Mehrdad Mahkam^b, Henrikki Liimatainen^{a,*}

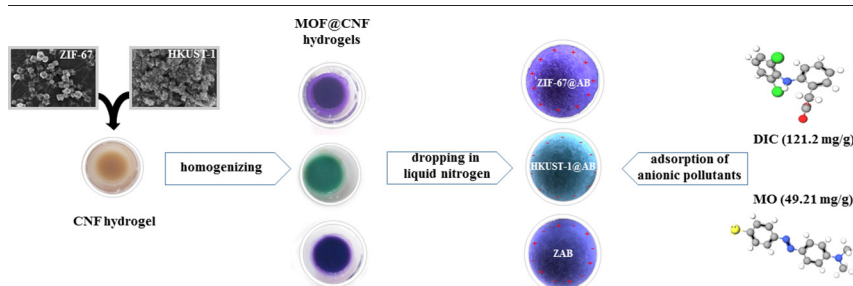
^a Fibre and Particle Engineering Research Unit, Faculty of Technology, University of Oulu, P.O. Box 4300, FI-90014, Finland

^b Department of Chemistry, Faculty of Science, Azerbaijan Shahid Madani University, P.O. Box 53714-161, Tabriz, Iran

HIGHLIGHTS

- A novel freeze-drying approach for fabrication of functional, highly porous nanocellulose aerobeads was introduced.
- Zwitterionic aerobeads were obtained by mixing of anionic (HKUST-1) and cationic (ZIF-67) MOFs in nanocellulose framework.
- The aerobeads showed an outstanding adsorption toward both diclofenac (121.20 mg/g) and methyl orange (49.21 mg/g).

GRAPHICAL ABSTRACT



ARTICLE INFO

Article history:

Received 24 May 2020

Received in revised form 26 August 2020

Accepted 26 August 2020

Available online 29 August 2020

Keywords:

Aerogel

Nanocellulose

Diclofenac

Methyl orange

Metal organic frameworks

ABSTRACT

Different adsorbents have been applied to remove various anionic pollutants in water treatment processes. However, the development of economic, sustainable, and high-performance adsorbents is still a challenge. Herein, we introduce a new strategy to produce highly porous (98.96%), very low density (0.015 g/cm^3), and cost-effective spherical and nanostructured hybrid aerogels, termed aerobeads, from cellulose nanofibers (CNF) and metal-organic frameworks (MOFs). The zwitterionic MOFs@CNF aerobeads (with 10–50 wt% MOF loading) were synthesized via simple dropping of a cross-linked hydrogel containing CNF and a binary mixture of anionic and cationic MOFs in liquid nitrogen, followed by freeze-drying. The flexible aerobeads (diameter of 2–3 mm) with hierarchical porous structure demonstrated an outstanding adsorption capacity toward both diclofenac (121.20 mg/g) and methyl orange (49.21 mg/g). Moreover, the aerobeads were easily collected after use from the solution without any complicated separation methods or the formation of secondary pollutants.

© 2020 The Author(s). Published by Elsevier Ltd. This is an open access article under the CC BY-NC-ND license (<http://creativecommons.org/licenses/by-nc-nd/4.0/>).

1. Introduction

In recent decades, toxic organic chemicals, which usually originate from various industries such as chemical companies, have polluted water resources and caused health problems. Most aqueous pollutants are in low concentrations, but they threaten drinkable water stocks and can cause serious ecological implications [1,2]. The emerging dye

and pharmaceutical pollutions with high mobility and toxic and carcinogenic effects can exacerbate mortality in plants, animals, and even humans [3]. For example, diclofenac (DIC), which is a commonly used anti-inflammatory drug, has been discovered in drinking water [4]. The fatal effects of DIC have been proven on the vultures of the Indian subcontinent and rainbow trout populations [5,6]. Besides the destructive effects of pharmaceutical pollutants, azo dyes (a class of dyes with azo groups (-N=N-), usually one to four, linked to phenyl and naphthyl radicals) emanating from different industries (e.g., textile, leather, paint, cosmetics, food, pharmaceutical, polymers, and additives in petroleum

* Corresponding author.

E-mail address: Henrikki.Liimatainen@oulu.fi (H. Liimatainen).

products) have detrimental effects on photosynthesis in aqueous media. Moreover, organic dyes are poorly biodegradable and spoil water resources due to negative effects on the photochemical activities [7–9]. Hence, increasing environmental concerns have highlighted the importance of economic, biodegradable, and efficient methods for eliminating aqueous dye and drug contaminations.

Numerous methods such as membrane filtration [10], oxidation processes [11], and adsorption [12] have been applied for removing water contaminants. In particular, adsorption techniques are often considered efficient, eco-friendly, feasible, and economical approaches for many water treatment purposes [13]. However, the elimination of highly persistent anionic micropollutants with current adsorbents [14] is challenging owing to the high polarity of contaminants and repulsive adsorbent-adsorbate charge interactions. Therefore, new adsorbents with high removal capacities to quickly remove aqueous anionic pollutants are highly desired.

Metal-organic frameworks, or MOFs, belong to a class of hybrid materials containing organic ligands and metal clusters with huge surface areas and crystalline structures. These materials with ultrahigh porosity typically have heterogeneous pore sizes, selective adsorption sites for the adsorbents, and high durability [15,16]. Due to these prominent characteristics, MOFs have been studied in various applications such as separation processes [17], catalysis [18], sensing [19], and drug delivery [20]. They have previously been used for the adsorption of gases and hazardous substances from aqueous media in particular [17]. MOFs have the ability to adsorb organic pollutants through various mechanisms such as H-bonding, π - π interactions, electrostatic forces, and hydrophobic and acid/base interactions [21]. For example, zirconium-based MOFs (UiO-66) with different functionalities have been used for the adsorption of methyl orange (MO) and methylene blue dyes via electrostatic and π - π interactions, as well as H-bonding [22]. Despite the many advantages of MOFs, they possess a notable practical drawback in water treatment as they exist in powder form, which makes their collection difficult and can create secondary pollutions [23]. Therefore, novel approaches to incorporate MOFs as a part of membranes [24], films [25], composites [26], and aerogels [27] have been harnessed to overcome the present defects of individualized MOF particles.

Aerogels are a class of hierarchical materials that are ultralightweight and have high surface area and porosity, besides very low density. Previously, mesoporous aerogels were combined with microporous MOFs to obtain hybrid nanomaterials [28]. In particular, the aerogels derived from cellulose nanomaterials offer an attractive, green, biodegradable, and tailorable medium to be combined with MOFs to design multifunctional materials. Earlier hybrids of nanocellulose aerogels and MOFs were used for the removal of Cr (VI) ions and bisphenol A [29].

In this study, we demonstrate an advanced concept for removing aqueous anionic micropollutants based on a novel type of spherical, hybrid, nanocellulose aerogel combined with a binary mixture of anionic and cationic MOFs. The spherical aerogels, termed aerobeads, are tailorable in size and surface chemistry and have even higher surface areas and adsorption capacities compared to their bulk counterparts [30]. To the best of our knowledge, binary MOF mixtures have previously been used only with chemo-resistive sensors to detect gas molecules [31]. Here, a zwitterionic porous hybrid design based on both cationic (ZIF-67) and anionic (HKUST-1) MOFs was engineered by crosslinking MOFs with a cationic cellulose nanofiber (CNF) hydrogel. The mixture was dropped in liquid nitrogen and freeze-dried to obtain zwitterionic MOFs@CNF aerobeads (i.e., ZABs). The performance of the aerobeads in removing DIC and MO was demonstrated in various conditions. ZAB particles showed excellent pH-sensitive adsorption of anionic contaminants. Moreover, they were easily collected manually without applying complicated methods. The present study designed a promising concept to incorporate MOFs in practical application by introducing them in highly porous nanocellulose aerogels. The results indicate the

potential of the hybrid adsorbent in wastewater treatment in particular. Moreover, the produced ultra-lightweight hybrids could potentially also be used in many other applications such as environmental conservation, electronic materials, catalysts, etc.

2. Experimental section

2.1. Materials

Collected waste boxboard was used as raw material for CNF fabrication. 1,3,5-benzenetricarboxylic acid (trimesic acid, 98%), 2-methylimidazole (2-MI, 98%), and diclofenac sodium salt (DIC) were purchased from Tokyo Chemical Industry Co. (TCI). Ethanol (99.9%), sodium hydroxide (0.1 M solution), hydrochloric acid (0.1 M solution), and dimethylformamide (technical grade) were obtained from VWR Co. Copper (II) hydroxide ($\text{Cu}(\text{OH})_2$, $\geq 98\%$) and cobalt (II) nitrate hexahydrate [$\text{Co}(\text{NO}_3)_2 \cdot 6\text{H}_2\text{O}$, 98–102%] were bought from Thermo Fisher. 3-chloro-2-hydroxypropyl trimethyl ammonium chloride (CHPTMAC, 60 wt% aqueous solution), methanol (99.9%), methyl orange (MO), and glutaraldehyde (25% aqueous solution) were delivered by Sigma-Aldrich Co.

2.2. Preparation of CNF from waste boxboard

Waste boxboard cellulose was first disintegrated using a Kenwood pulper (KM020, UK) at a 1/min rotor speed (consistency of 15 wt%), washed, and then sieved using a screen (Somerville, Lorentzen & Wettre, Sweden). The cellulose was nanofibrillated with an MKCA6-2J grinder (Masuko super masscolloider, Japan) to produce aqueous CNF gel. Briefly, disks of the grinder were brought in near distance of each other to pass the diluted cellulose pulp (1.5 wt%) through Masuko disks with zero disks gaps (3 times). The negative gaps (–20, –40, –50, –60, –80, and –90 μm) of the disks were then set, and the pulp was passed 17 times more through the disks. Transmission electron microscopy (TEM) showed successful preparation of cellulose nanofibers (Supplementary Fig. S1).

2.3. Synthesis of metal-organic frameworks (ZIF-67 and HKUST-1)

Metal organic frameworks were synthesized at room temperature according to the previously reported methods [32–34]. Cationic ZIF-67 was fabricated by adding 4 mmol $\text{Co}(\text{NO}_3)_2 \cdot 6\text{H}_2\text{O}$ to 16 mmol 2-MI (each one in 100 mL methanol) and mixing at room temperature for 2 h. For synthesis of anionic HKUST-1, aqueous $\text{Cu}(\text{OH})_2$, and trimesic acid (in DMF and ethanol) was mixed at room temperature for 5 min (Cu:trimesic acid:DMF:ethanol: H_2O mole ratio was 1:1:12.9:80:100). The synthesized MOFs were centrifuged in absolute ethanol at 9092 rpm ($10,000 \times G$) for 10 min at 5 °C and then dried in an oven at 60 °C for 48 h.

2.4. Modification of cellulose nanofibers

The nanofibers were first functionalized with amine groups and then cross-linked with glutaraldehyde to increase the stability of the aerogels. Cationic CNF (CNF^+) was synthesized according to the literature [35,36] by adding 6 mL of CHPTMAC to 50 mL of aqueous solution of sodium hydroxide (4 wt%), mixing for 30 min, and then dosing CNF (1.25 g nanocellulose, 1 wt%) to the above solution followed by stirring for 24 h. The cationic CNF suspension was adjusted to a pH of 7 after filtering and was washed several times with deionized water. Cross-linked nanocellulose was prepared with the modified method reported by Zhu et al. [37]. Glutaraldehyde (6 v/v%) was added to the aqueous 0.5 wt% cationic CNF suspension under magnetic stirring at 65 °C in acidic media (pH = 3) for 6 h. The product was then filtered, washed, and diluted to 1 wt%.

Table 1
Composition, porosity, and density of the prepared aerobeads.

Sample	CNF (wt%)	ZIF-67 (wt%)	HKUST-1(wt%)	Porosity (%)	Density (g/cm ³)
AB	100	–	–	98.96	0.015
ZIF-67@AB (10%)	90	10	–	98.63	0.020
ZIF-67@AB (30%)	70	30	–	98.25	0.026
ZIF-67@AB (50%)	50	50	–	97.90	0.032
HKUST-1@AB (10%)	90	–	10	98.71	0.019
HKUST-1@AB (30%)	70	–	30	98.18	0.027
HKUST-1@AB (50%)	50	–	50	97.61	0.036
ZAB (10%)	90	5	5	98.62	0.016
ZAB (30%)	70	15	15	98.37	0.024
ZAB (50%)	50	25	25	98.27	0.026

2.5. Preparation of ZAB aerobeads

ZIF-67 and HKUST-1 particles with different concentrations were premixed with the modified CNF mixture (1 wt%) for 5 min and then sonicated using a probe sonicator for 15 min (Table 1). First HKUST-1 was added and homogenized with the nanocellulose hydrogels, and then ZIF-67 was dosed (pH = 6.5). A scheme for the fabrication of ZAB hydrogels is shown in Fig. 1. The homogenized MOF-CNF mixture was filled inside a syringe (0.5 mm tip diameter) and then dropped in the liquid nitrogen. The frozen aerobeads were dried at $-54\text{ }^{\circ}\text{C}$ using a Scanvac Coolsafe freeze-dryer (55-15 Pro, Denmark) for 72 h. The zwitterionic MOFs@CNF aerobeads were named ZAB, pure aerobeads without any MOFs were coded as AB, and aerobeads containing either ZIF-67 or HKUST-1 were named ZIF-67@AB and HKUST-1@AB, respectively. All MOF containing aerobeads were prepared in three different MOF/CNF ratios (i.e., 10, 30, and 50 wt%).

2.6. Porosity and density of aerobeads

The porosity (P) and density (ρ) of the aerobeads were determined according to Eqs. (1) and (2).

$$P = \frac{V - \left(\frac{m}{\rho_c}\right)}{V} \quad (1)$$

where V and m are volume (cm³) and mass (g) of aerobeads, respectively, and ρ_c is density of the bulk cellulose (1.528 g/cm³).

$$\rho = \frac{m}{V} \quad (2)$$

The volume of aerobeads was determined using an optical microscope, and mass was weighed using a laboratory balance (Mettler Toledo, XP6 model, Switzerland).

2.7. Fourier transform infrared (FTIR) spectroscopy

Cellulose nanofiber samples were analyzed with a Bruker FT-IR spectrometer (Germany). The samples (2 mg) were dried in an oven and crushed to powder form and then mixed with dry KBr (200 mg).

2.8. X-ray diffractometry (XRD)

The XRD patterns of the MOF particles were recorded with a Rigaku Smart Lab XRD instrument (Japan) in a continuous scan mode with a five-axis θ - θ goniometer then compared with the database of powder diffraction patterns.

2.9. Thermogravimetric analysis (TGA)

The aerobeads were analyzed with a Netzsch STA 409PC thermal analyzer (Germany). Each measurement was performed with the freeze-dried nanofibrillated sample in a DSC-Cp (i.e. platinum-corundum sample carrier with S-type thermocouples) under dry air atmosphere (approximately 60 mL/min), which was heated from 25 to 600 $^{\circ}\text{C}$.

2.10. Field emissions scanning electron microscopy (FESEM)

A carbon-coated holder was used for imaging aerobeads with the Ultra Plus instrument (Zeiss, Germany). Briefly, a thin aerogel specimen with the presence or absence of MOFs was put on the carbon surface of the holder and sputtered with platinum before being imaged at 5 kV.

2.11. Transmission electron microscope (TEM)

The cellulose nanofiber structure was investigated using the JEOL JEM-2200FS TEM (Japan) instrument. A small drop of diluted CNF suspension was put on the copper-coated grid, and then excess water drops were eliminated with a filter paper. The CNF sample was then negatively stained by placing a droplet of uranyl acetate (2% w/v) on top of each specimen. The excess amount of uranyl acetate was removed with a small filter paper, and the sample was dried at room temperature before being used for imaging at 200 kV.

2.12. Brunauer-Emmett-Teller (BET) analysis

The N₂ adsorption-desorption was analyzed at -195 to $-196\text{ }^{\circ}\text{C}$ with a micromeritics instrument. The aerobeads and MOF particles were degassed before analysis at 75 $^{\circ}\text{C}$ to eliminate all impurities.

2.13. Water uptake test

Water uptake of the aerobeads was analyzed similarly to our previous work [30]. In brief, approximately 40 mg of aerobeads was immersed in 50 mL deionized water (DI) for 1 min and then weighed quickly. The water uptake was calculated with Eq. (3):

$$K = \frac{W - W_0}{W_0} \quad (3)$$

where W_0 and W are the weight of the aerobeads before and after water uptake, respectively.

2.14. Stability test

The mechanical stability of aerobeads was tested in three different pH (5, 6.5, and 8). A pre-determined amount of each aerobead was soaked in water with different pH for 1 min and weighted immediately.

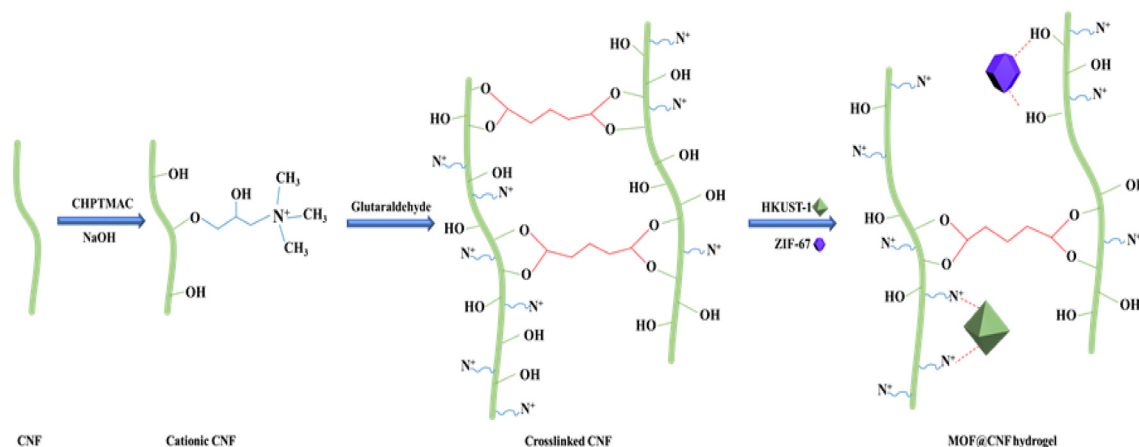


Fig. 1. A schematic overview for the synthesis of ZAB hydrogels.

The wet aerobeads were submerged again in the aqueous media and were exposed for shaking (120 rpm) and were weighed for the second time after desired time (1–6 h). The weight retention of aerobeads were calculated using the Eq. (4):

$$\text{Weight retention} = \frac{W_t}{W_0} \quad (4)$$

where, W_0 and W_t are the wet weights of the hydrogels before and after shaking.

2.15. Adsorption test

Adsorption experiments on the aerogels with anionic micropollutants (DIC and MO) were conducted by shaking the scaled amount of aerobeads in 10 mL of pollutant solution at 100 rpm for 24 h. To explore the effects of pH, contact time, and pollutant concentration on adsorption capacity, the experiments were conducted in different conditions. The aerobeads were collected manually after adsorption, and the adsorption capacities of DIC and MO were determined using a UV-vis spectrophotometer (Shimadzu, Japan) at 276 and 464 nm wavelengths, respectively. The adsorption capacity was calculated by Eq. (5):

$$q_t = \frac{(C_0 - C_t)V}{m} \quad (5)$$

where C_0 and C_t are the concentrations of the initial solution at time t (mg/L), respectively. V is pollutant solution volume (L), m is aerobead mass (g), and q_t is adsorption capacity (mg/g) of aerobeads at time t .

To analyze the kinetics of the pollutant's removal, pseudo-first-order (Eq. (6)) and second-order (Eq. (7)) models were used for both MO and DIC.

$$\ln(q_e - q_t) = \ln q_e - k_1 t \quad (6)$$

$$\frac{t}{q_t} = \frac{1}{K_2 q_e^2} + \frac{t}{q_e} \quad (7)$$

where q_e is the adsorption capacity in equilibrium; k_1 and k_2 are the first- and second-order kinetic constant, respectively.

3. Results and discussion

3.1. Engineering of MOF@CNF aerobeads

The synthesis of zwitterionic aerobeads was performed through the cationization and crosslinking of CNFs, mixing of anionic and cationic MOF crystals with the modified CNF hydrogel and dropping the mixture

in the liquid nitrogen, followed by freeze-drying. The cationization of CNF was used to both improve the loading of anionic MOFs in the aerobeads and enhance the interaction of aerobeads toward anionic micropollutants as depicted in the Fig. 1. To facilitate the stability of aerobeads in aqueous media, the cationic CNF hydrogels were cross-linked with glutaraldehyde through hydroxyl groups [37]. Previously, the maximum MOF loading of 50 wt% was obtained with the CNF aerogels [23]. Here, the maximum total dosage of cationic (ZIF-67) and anionic (HKUST-1) MOFs was also set to 50 wt%. Despite some previous studies using organic solvents to fabricate materials containing CNF and MOFs [28], all of the process steps were conducted in water.

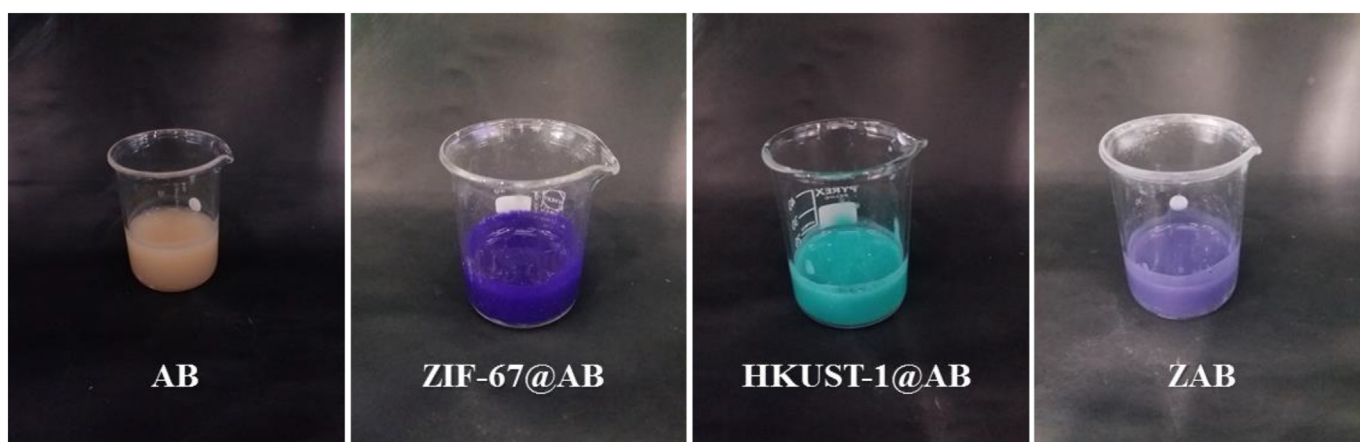
3.2. Characterization of MOF@CNF aerobeads

The spherical aerobeads were created via dropping the MOF@CNF hydrogel mixture in liquid nitrogen. As shown in Fig. 2, the MOF crystals were suspended homogeneously in the CNF hydrogel matrix after sonication. The aerobeads exhibited a uniform size of 2–3 mm and symmetrical shape, indicating the reproducibility of the dropping method.

Because of the poor stability of aerobeads with MOFs loading higher than 50 wt%, the MOF@CNF aerobeads were prepared only in three and up to 50 wt% total weight ratios of MOFs, i.e. 10, 30, and 50 wt% (Table 1). All the aerobeads demonstrated very high porosity, ranging from 97.61 to 98.96%, and low densities of 0.015–0.036 g/cm³. The increase of MOF loading only slightly decreased the porosity, but increased the density of the aerobeads >100% at the highest MOF dosage. However, the MOF particles insertion in the aerobeads did not have major effects on the other physical properties of the aerobeads.

ZIF-67 and HKUST-1 crystals with rhombic dodecahedral and octahedral structures as determined by FESEM are shown in Fig. 3a and b, respectively. The images proved the monodispersed shape and sharp edges of MOF particles with an average size of 800 nm (ZIF-67) and 300 nm (HKUST-1). The size of the ZIF MOFs can be affected by adjusting interactions between the metal ion and ligands through changing the type of salt used [38]. By applying cobalt nitrate salt, ZIF-67 particles of less than 1 μm were obtained. Unlike most of the reported synthesis methods, HKUST-1 was prepared under ambient temperature and in a water/ethanol solution. However, prepared HKUST-1 crystals had the same framework structure as typically obtained by the solvothermal method [34].

FESEM images illustrate that the MOF crystals were dispersed homogeneously without any agglomeration in the interspace network of CNF. In addition, the MOFs were partly embedded in the thin layers formed by the cellulose nanofiber network. The hydrogen bonding between the CNF and MOF presumably promoted adhesion between the constituents (Fig. 3d–f).



Dropping in liquid nitrogen

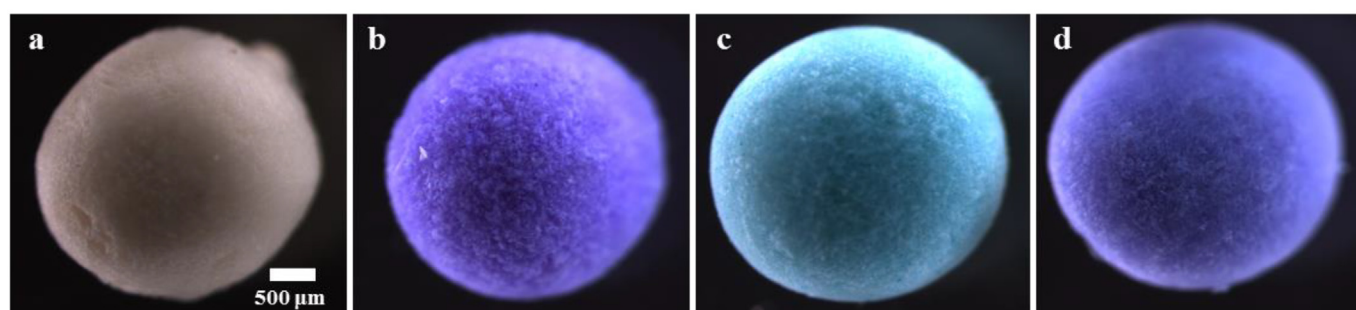


Fig. 2. Optical microscopic images of a) AB, b) ZIF-67@AB (30%), c) HKUST-1@AB (30%), and d) ZAB (30%) hydrogels (up) and aerobeads (down).

The FT-IR spectra of original CNF, cationic CNF (CNF⁺), and cross-linked CNF (C-CNF) are shown in Fig. 4a. The CNF presented peaks at 2860–2900 cm⁻¹, 3400 cm⁻¹, and 1000–1100 cm⁻¹ allocated to C–H, hydroxyl, and C–O bonds, respectively [36,39]. A peak of the CNF⁺ at 1481 cm⁻¹ was attributed to methyl groups in the quaternary

ammonium [40,41]. The hydroxyl groups of CNF and aldehyde groups of glutaraldehyde molecules were cross-linked via C–O bonds. This acetate crosslinking interaction can be detected in the FT-IR spectra of C-CNF at 1710 cm⁻¹ [37]. Moreover, the crystallinity and also the purity of the synthesized MOFs were proved by XRD analysis (Fig. 4b). The

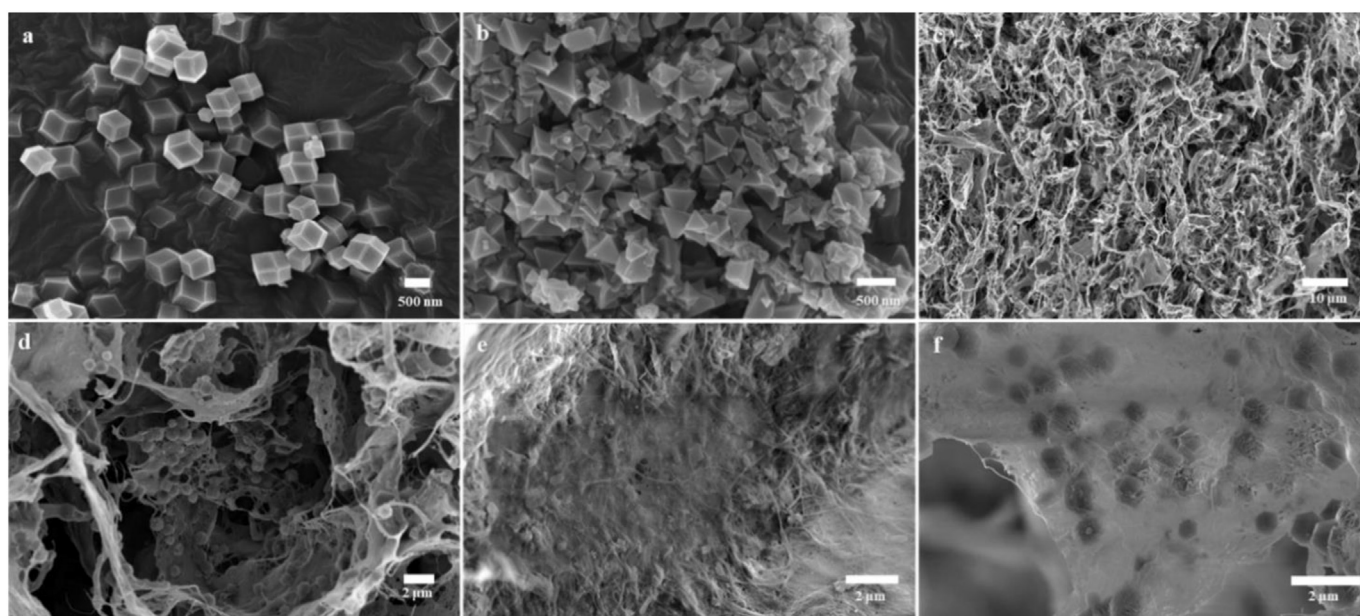


Fig. 3. SEM images of a) ZIF-67, b) HKUST-1 MOF crystals, c) CNF, d) ZIF-67@AB (30%), e) HKUST-1@AB (30%), and f) ZAB (30%).

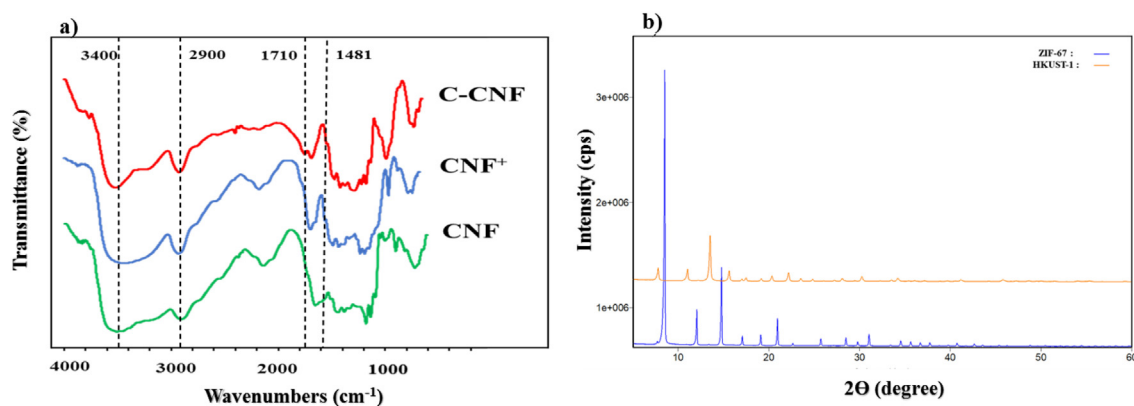


Fig. 4. a) FT-IR spectra of CNF, cationic CNF (CNF⁺), and cross-linked CNF (C-CNF), and b) XRD patterns of ZIF-67 and HKUST-1 MOFs.

presence of strong and sharp peaks at 8.51°, 12.05, 14.78, 17.08, 19.1, and 24.25 in the XRD patterns reflect the desirable crystallinity of ZIF-67 particles. This result match well with the recently reported studies [32]. HKUST-1 was synthesized with the conversion of insoluble copper hydroxide into HKUST-1 at room temperature. The XRD results proved the stability and high crystallinity of the synthesized HKUST-1. In addition, the crystalline structure of HKUST-1 was similar to that in the previous reports [33,34]. No distinct impurity peaks were determined in the HKUST-1 XRD patterns.

Isotherm linear plots for the adsorption-desorption of N₂ for the prepared aerobeads (i.e., AB, HKUST-1@AB (30%), ZIF-67@AB (30%), and ZAB (30%)) and MOFs (HKUST-1 and ZIF-67) are shown in Supplementary Fig. S2. Adsorption average pore widths (4 V/A by BET) of ZAB, ZIF-67@AB (30%), and HKUST-1@AB (30%) were 1.2 nm, 3.7 nm, and 12.2 nm, respectively. BET surface area of cellulose aerobeads (AB) increased by introducing MOF particles in their porous structures. For instance, surface area of ZAB (30%) (125 m²/g) was 3 times higher than that of AB microspheres (41 m²/g).

The TGA of the CNF aerobeads without MOFs (AB) and zwitterionic aerobeads having variable content of MOFs are shown in Fig. 5. The appropriate incorporation of MOFs in the aerobeads formulation can be explained with TGA analysis by the consistent weight loss of aerobeads. The decrease in the aerobeads' weight at 220 °C is presumably attributed to degradation of the cellulose structure. Subsequently, the significant mass loss of aerobeads at >300 °C was associated with the degradation of MOF structure caused by the disjoining of ligand structures [23,28,32].

3.3. Adsorption behavior and removal of anionic micropollutants using MOF@CNF aerobeads

First, the water uptake capacity of the aerobeads was analyzed in an immersion test (Fig. 6). The water uptake of the aerobeads ranged between 39.7 and 60.6 g/g, and the increase in the MOFs dosage in CNF aerogels structure decreased the water uptake. However, the adsorption capacity of ZAB with the highest MOF dosage of 50% was still at a good level (75% of capacity of AB) and comparable to what has been previously reported for the flexible aerogels from cellulose nanofibers [42]. The high water uptake capacity is associated with the unique spherical and highly porous design of the aerogels. Such a desirable performance of aerobeads might be conducive for adsorbing of the targeted micropollutants. [43,44]. The hierarchical mesoporous structure of an adsorbent can contribute to both capacity and speed of removing pollutants [45]. The freeze-dried aerobeads had interconnected, millimeter size, and porous (porosity more than 98%) structures which enable them to accumulate and transfer the water-soluble pollutants.

The freeze-dried aerobeads were stable in the aqueous media. It was likely attributed to chemical crosslinking used in the nanocellulose structure. For example, the maximum degradation of ZAB 30 (30%) after 6 h was less than 9% of aerobeads weight. The initial loss of aerobeads weight might be associated with the surface corrosion of the aerobeads (Supplementary Fig. S5).

DIC and MO with the ZAB, ZIF67@AB, HKUST-1@AB, and reference aerobeads were monitored at 25 °C at different pHs (5, 6.5, and 8) using a constant micropollutant dosage of 10 ppm (Fig. 7a and

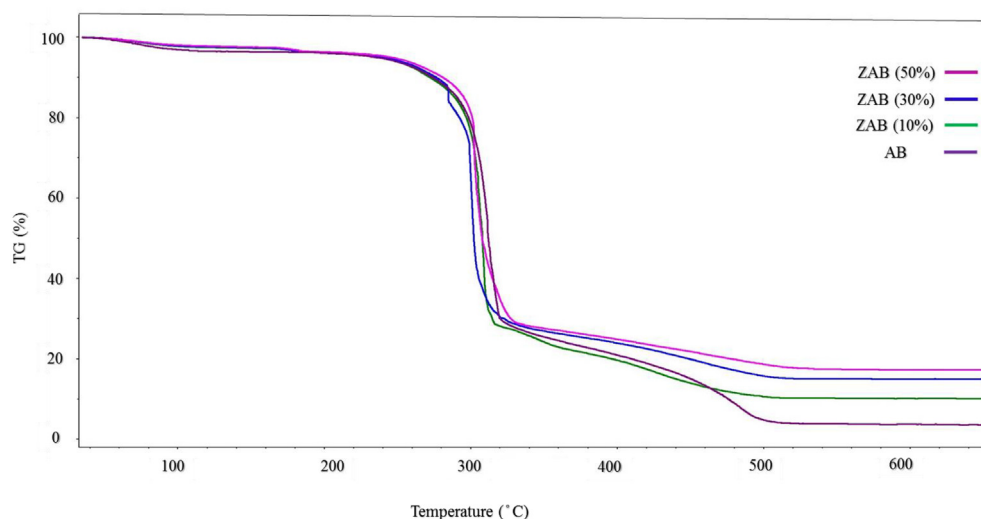


Fig. 5. TGA curve of AB, ZAB (10%), ZAB (30%), and ZAB (50%).

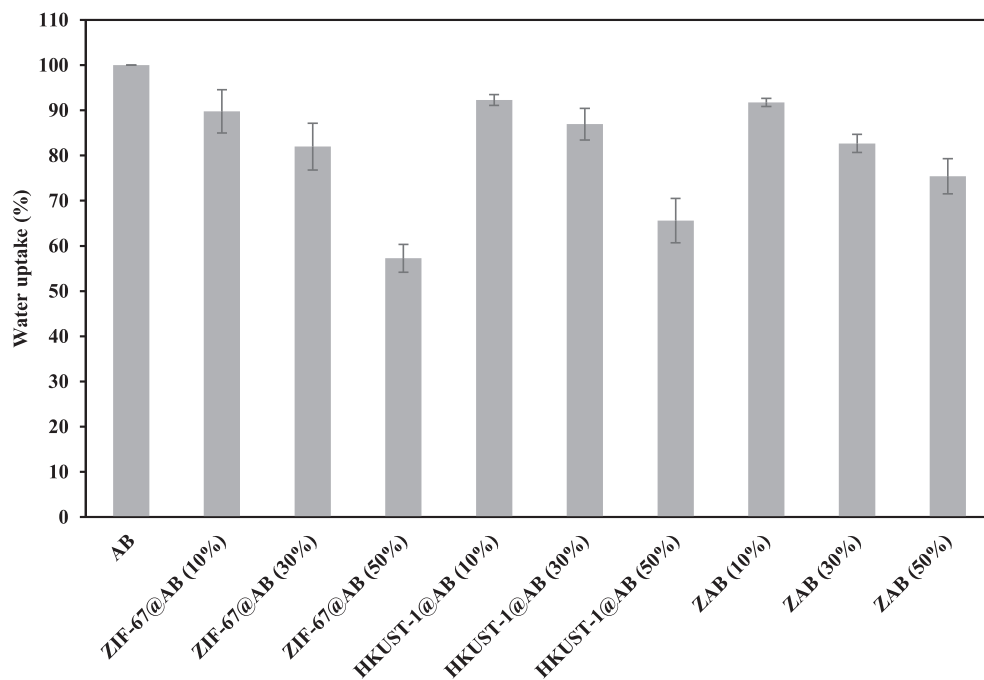


Fig. 6. Water uptake capacity (%) of the aerogels.

b). The MOF containing aerogels showed better adsorption performance than that of the reference aerogels (without any MOFs). It was likely that micropollutants (i.e. DIC and MO) adsorbed on aerogels through hydrogen bonding. In addition, DIC and MO with electronegative atoms such as N and O can be adsorbed strongly by opposite groups of the MOFs. On the other hand, the solution pH has an intrinsic role in hydrogen bonding and adjusts the deprotonation/protonation in the adsorbent. Therefore effects of the solution pH on the adsorption of DIC and MO were addressed. The adsorption (q_t) for both DIC and MO pollutants using zwitterionic aerogels in pH 8 were higher than other aerogels, indicating the successful formulation of ZABs. Interestingly, HKUST-1@AB adsorbed DIC at pH 5 around twice as much as pure aerogels. This behavior might be attributed to strong H-bonding between carboxyl groups of adsorbent and DIC molecules. However, the highest adsorption capacity of DIC (i.e., 121.20 mg/g) was observed with ZIF-67@AB (50%) at pH 6.5. Such high adsorption of anionic pollutants is likely associated with the positive surface charge of ZIF-67, which promotes the adsorption of anionic DIC via electrostatic forces [46,47]. Clearly, aerogels with a 50 wt% loading amount of MOFs showed a better adsorbing performance than that of reference aerogels. This result showed that micropollutant uptake was a surface dependent phenomenon. The adsorption capacity of MO varied from 14.33–49.21 mg/g, and the highest was for ZAB (50%) (Fig. 7b). The outstanding adsorption capacity might pertain to the homogeneous distribution of nanoporous, zwitterionic MOF particles in the hierarchical and interconnected structure of spherical aerogels. In general, the existence of nano/microporous structure strongly enhance the selective adsorption of pollutants [48]. Moreover, the imidazole and benzene rings of ZIF-67 and HKUST-1 might improve the adsorbing performance via π - π interactions with aromatic rings. ZAB particles were gathered from the aqueous solution manually without using any intricate procedure.

To better understand the adsorption performance of MOF-containing aerogels, the kinetics of adsorption of DIC and MO at an adsorption dosage of 10 ppm was investigated (Fig. 8 and Supplementary Fig. S4). The adsorption was relatively slow, and the plateau adsorption was reached after >200 min with all samples. It was also reported previously that the microporous adsorbents require a long time to reach an

equilibrium [49]. Considering the empirical results of adsorption and correlation factors, the pseudo-second-order model resulted in the best fit between observed and theoretical amounts. The correlation coefficients (R^2) for the pseudo-second-order model were between 0.97

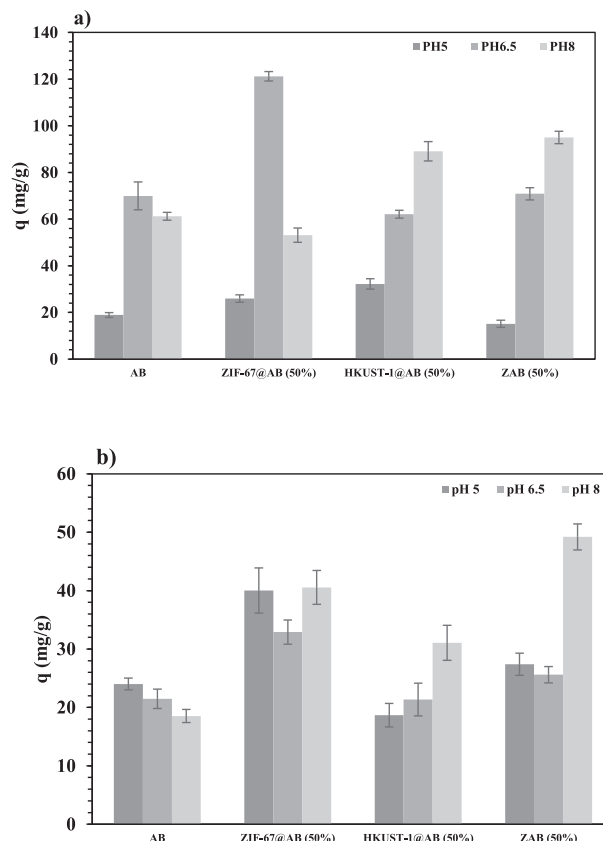


Fig. 7. Adsorption of a) DIC and b) MO with aerogels at pH 5, 6.5, and 8.

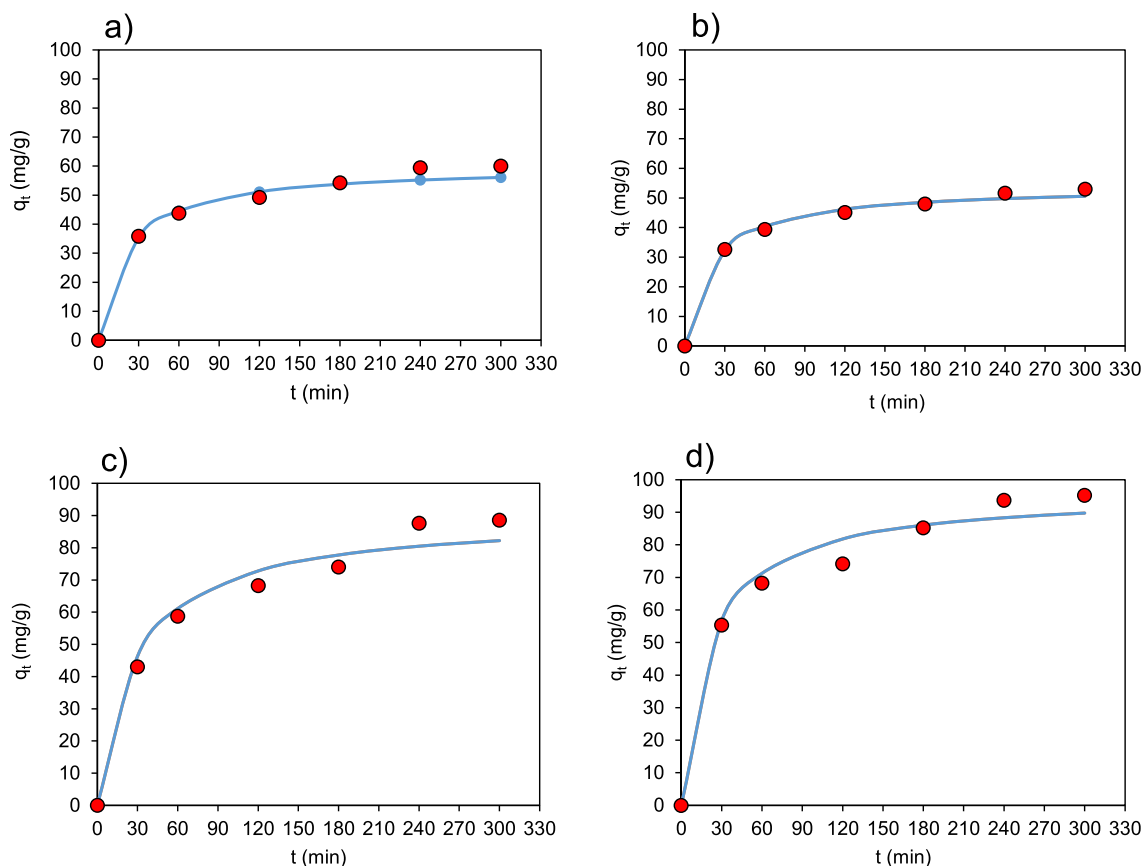


Fig. 8. Data fitting for adsorption of DIC by a) AB, b) ZIF-67@CNF (50%), c) HKUST-1@CNF (50%), and d) ZAB (50%) as a function of time at pH = 8 with pseudo-second-order equation.

and 0.99 for DIC and more than 0.99 for MO (Supplementary Table S1). Therefore, the results indicated that the micropollutant uptake was based on chemical sorption [50].

The adsorption capacity in most of the prepared aerobeads varied significantly as a function of pH, meaning that surface charges in the aerobeads is pH-dependent. As shown in Supplementary Fig. S3, the charge density of the aerobeads decreased as the pH raised from 3 to 10. In basic pH, deprotonation of acidic groups and also surrounding the positive charges might explain this effect. The previous reports of charge density of cellulose nanofibers also support the pH-dependent charge behavior [51].

3.4. Comparison of different adsorbents in removal of anionic micropollutants

Recently, many adsorbents have been introduced for the elimination of anionic micropollutants, including MO and DIC (Table 2). When comparing the ZAB adsorbents with the previously reported adsorbents, a

very high adsorption capacity (121.20 mg/g for DIC and 49.21 mg/g for MO) was reached in the present study, especially with DIC, the maximum capacity with ZAB (50%) being higher than that in previous works. Earlier, the DIC removal with the carbon xerogel, ZIF-8, modified cellulosic filter paper, and wood-based filtration device were 80, 100, 25, and 178.6 mg/g respectively [49,52–54]. The adsorption capacity with MO was similar to PPy/SBA-15 nanocomposite, but smaller than that of UiO-66-NH₂ (MOF). Bulk nanocellulose aerogels in combination with MOFs have previously been used for the selective removal of cationic dyes [55] and cationic Cr (VI) [29] with high adsorbing capacity, but reports related to the use of cellulose nanomaterials and MOFs for removing anionic micropollutants are lacking. The high capacity is likely associated with homogenous dispersion of MOFs in interconnected spaces of CNF microspheres, high adsorbent-adsorbate affinity, and also the high surface area of the spherical aerobeads. The prepared ZABs overcome many typical drawbacks, such as complicated and poisonous synthesis methods and difficult separation of the powder adsorbents from the aqueous suspensions associated to previous adsorbents.

Table 2
Comparison of the adsorption capacities of recently reported adsorbents.

Year (ref)	Type of adsorbent	pollutant	MOF (% wt)	Adsorption (mg. g ⁻¹)
2015 [49]	Carbon xerogel	DIC	–	80
2017 [53]	ZIF-8 (MOF)	DIC	–	100
2019 [52]	Cyclodextrin-cellulose filter paper	DIC	–	25
2020 [54]	Wood@MIL-101(Fe) membrane	DIC	–	178.6
Present work	MOF@CNF aerobead	DIC	10–50	121.20
2018 [57]	PPy/SBA-15 nanocomposite	MO	–	41.66
2019 [22]	UiO-66-NH ₂ (MOF)	MO	–	148.4
Present work	MOF@CNF aerobead	MO	10–55	49.21

Concerning the pH of municipal wastewaters (6.5–8), these adsorbents could be optimal for wastewater cleaning applications. The novel processing procedure and employing influential materials could decrease the cost price of cleaner products named as low-cost sorbents. The components of these adsorbents might be a natural byproduct or waste materials. Therefore a fast looking up to the price of nanocellulose realizes the importance of using waste boxboard cellulose (80–100 €) instead of virgin birch cellulose (600–800 €) in aerobeads structure [56].

The spherical aerobeads were easily separated manually without complicated methods after adsorbing micropollutants from water solutions. The aerobeads remained their spherical shape and mechanical stability without structural collapse during the adsorption process. After drying the used aerobeads, they were still in good shape and could be used for at least three times more. However, cracks were appeared in the surface of beads after multiple use. Therefore, the binary MOFs and CNF aerobeads with high porosity, ultra-low density, facile synthesis, and high adsorption performance were developed as a high-potential nanostructured adsorbent for the removal of anionic pollutants.

4. Conclusions and perspectives

A combination of two MOFs with CNF was applied to produce spherical and nanoporous hybrid adsorbents. For the first time, the advanced design for stabilizing binary MOFs inside aerogels were conducted, and aerobeads with zwitterionic properties synthesized. The binary MOF containing aerobeads showed a very high adsorbing capacity to remove two important anionic pollutants (121.20 mg/g for DIC and 49.21 mg/g for MO). The aerobeads were easily collected after use from the solution without any complicated separation methods or the formation of secondary pollutants. The produced hybrid adsorbents are cost-effective, environmentally-friendly and they can be produced via facile synthesis route.

Credit author statement

Mohammad Karzar Jeddi participated in experimental design and conducted the experiments and prepared the first draft of the manuscript. Ossi Laitinen and Henriikki Liimatainen participated in experimental design, supervision of the experimental work and writing and finalization of the manuscript. Mehrdad Mahkam participated in supervision of the work.

Declaration of Competing Interest

None.

Acknowledgement

This research was supported by grants from the Academy of Finland projects “Bionanochemicals” (No. 298295) and “ACNF—Functional nanoribbons from asymmetrically modified cellulose nanomaterials” (No. 325276). Mr. Tommi Kokkonen is acknowledged for his kind assistance for the TGA measurements from the Centre for Advanced Steels Research of the University of Oulu. We would like to also thank Ms. Heini Tuorila for improving the graphical abstract.

Appendix A. Supplementary data

Supplementary data to this article can be found online at <https://doi.org/10.1016/j.matdes.2020.109106>.

References

- [1] A. Bo, S. Sarina, H. Liu, Z. Zheng, Q. Xiao, Y. Gu, G.A. Ayoko, H. Zhu, Efficient removal of cationic and anionic radioactive pollutants from water using hydrotalcite-based getters, *ACS Appl. Mater. Interfaces* 8 (2016) 16503–16510, <https://doi.org/10.1021/acsami.6b04632>.
- [2] J.F.J.R. Pesqueira, M.F.R. Pereira, A.M.T. Silva, Environmental impact assessment of advanced urban wastewater treatment technologies for the removal of priority substances and contaminants of emerging concern: a review, *J. Clean. Prod.* 261 (2020) 121078, <https://doi.org/10.1016/j.jclepro.2020.121078>.
- [3] S. Yu, X. Wang, H. Pang, R. Zhang, W. Song, D. Fu, T. Hayat, X. Wang, Boron nitride-based materials for the removal of pollutants from aqueous solutions: a review, *Chem. Eng. J.* 333 (2018) 343–360, <https://doi.org/10.1016/j.cej.2017.09.163>.
- [4] T. Heberer, Tracking persistent pharmaceutical residues from municipal sewage to drinking water, *J. Hydrol.* 266 (2002) 175–189, [https://doi.org/10.1016/S0022-1694\(02\)00165-8](https://doi.org/10.1016/S0022-1694(02)00165-8).
- [5] J. Schwaiger, H. Ferling, U. Mallow, H. Wintermayr, R.D. Negele, Toxic effects of the non-steroidal anti-inflammatory drug diclofenac, *Aquat. Toxicol.* 68 (2004) 141–150, <https://doi.org/10.1016/j.aquatox.2004.03.014>.
- [6] J. Hofmann, U. Freier, M. Wecks, S. Hohmann, Degradation of diclofenac in water by heterogeneous catalytic oxidation with H₂O₂, *Appl. Catal. B Environ.* 70 (2007) 447–451, <https://doi.org/10.1016/j.apcatb.2005.11.023>.
- [7] X. Wang, W. Zhou, C. Wang, Z. Chen, Cotton fiber-supported layered double hydroxides for the highly efficient adsorption of anionic organic pollutants in water, *New J. Chem.* 42 (2018) 9463–9471, <https://doi.org/10.1039/C8NJ00678D>.
- [8] X. Liu, L. Huang, D. Zhang, T. Yan, J. Zhang, L. Shi, Light driven fabrication of highly dispersed Mn-Co/RGO and the synergistic effect in catalytic degradation of methylene blue, *Mater. Des.* 140 (2018) 286–294, <https://doi.org/10.1016/j.matdes.2017.11.057>.
- [9] R. Li, X.J. Liu, H. Wang, Y. Wu, K.C. Chan, Z.P. Lu, Flexible glassy grid structure for rapid degradation of azo dye, *Mater. Des.* 155 (2018) 346–351, <https://doi.org/10.1016/j.matdes.2018.06.022>.
- [10] F. Albertini, T. Ribeiro, S. Alves, C. Baleizão, J.P.S. Farinha, Boron-chelating membranes based in hybrid mesoporous silica nanoparticles for water purification, *Mater. Des.* 141 (2018) 407–413, <https://doi.org/10.1016/j.matdes.2018.01.001>.
- [11] P. Xu, H. Han, H. Zhuang, B. Hou, S. Jia, C. Xu, D. Wang, Advanced treatment of biologically pretreated coal gasification wastewater by a novel integration of heterogeneous Fenton oxidation and biological process, *Bioresour. Technol.* 182 (2015) 389–392, <https://doi.org/10.1016/j.biortech.2015.02.019>.
- [12] Q. Lv, X. Hu, X. Zhang, L. Huang, Z. Liu, G. Sun, Highly efficient removal of trace metal ions by using poly(acrylic acid) hydrogel adsorbent, *Mater. Des.* 181 (2019), 107934 <https://doi.org/10.1016/j.matdes.2019.107934>.
- [13] M. Cantarella, S.C. Carroccio, S. Dattilo, R. Avolio, R. Castaldo, C. Puglisi, V. Privitera, Molecularly imprinted polymer for selective adsorption of diclofenac from contaminated water, *Chem. Eng. J.* 367 (2019) 180–188, <https://doi.org/10.1016/j.cej.2019.02.146>.
- [14] B. Yu, Z. Li, H. Cong, G. Li, Q. Peng, C. Yang, Synthesis and application of sulfonated polystyrene/ferrosulfate oxide/diazo resin nanocomposite microspheres for highly selective removal of dyes, *Mater. Des.* 135 (2017) 333–342, <https://doi.org/10.1016/j.matdes.2017.09.039>.
- [15] J. Ren, X. Doyosiba, N.M. Musyoka, H.W. Langmi, M. Mathe, S. Liao, Review on the current practices and efforts towards pilot-scale production of metal-organic frameworks (MOFs), *Coord. Chem. Rev.* 352 (2017) 187–219, <https://doi.org/10.1016/j.ccr.2017.09.005>.
- [16] P. Brandt, A. Nuhnen, M. Lange, J. Möllmer, O. Weingart, C. Janiak, Metal-organic frameworks with potential application for SO₂ separation and flue gas desulfurization, *ACS Appl. Mater. Interfaces* 11 (2019) 17350–17358, <https://doi.org/10.1021/acsami.9b00029>.
- [17] N.A. Khan, Z. Hasan, S.H. Jung, Adsorptive removal of hazardous materials using metal-organic frameworks (MOFs): a review, *J. Hazard. Mater.* 244–245 (2013) 444–456, <https://doi.org/10.1016/j.jhazmat.2012.11.011>.
- [18] J. Liu, L. Chen, H. Cui, J. Zhang, L. Zhang, C.-Y. Su, Applications of metal-organic frameworks in heterogeneous supramolecular catalysis, *Chem. Soc. Rev.* 43 (2014) 6011–6061, <https://doi.org/10.1039/C4CS00094C>.
- [19] P. Kumar, A. Deep, K.-H. Kim, Metal organic frameworks for sensing applications, *TrAC Trends Anal. Chem.* 73 (2015) 39–53, <https://doi.org/10.1016/j.trac.2015.04.009>.
- [20] P. Horcajada, T. Chalati, C. Serre, B. Gillet, C. Sebrie, T. Baati, J.F. Eubank, D. Heurtaux, P. Clayette, C. Kreuz, J.-S. Chang, Y.K. Hwang, V. Marsaud, P.-N. Bories, L. Cynober, S. Gil, G. Férey, P. Couvreur, R. Gref, Porous metal-organic-framework nanoscale carriers as a potential platform for drug delivery and imaging, *Nat. Mater.* 9 (2010) 172–178, <https://doi.org/10.1038/nmat2608>.
- [21] Z. Hasan, S.H. Jung, Removal of hazardous organics from water using metal-organic frameworks (MOFs): plausible mechanisms for selective adsorptions, *J. Hazard. Mater.* 283 (2015) 329–339, <https://doi.org/10.1016/j.jhazmat.2014.09.046>.
- [22] S.-W. Lv, J.-M. Liu, H. Ma, Z.-H. Wang, C.-Y. Li, N. Zhao, S. Wang, Simultaneous adsorption of methyl orange and methylene blue from aqueous solution using amino functionalized Zr-based MOFs, *Microporous Mesoporous Mater.* 282 (2019) 179–187, <https://doi.org/10.1016/j.micromeso.2019.03.017>.
- [23] H. Zhu, X. Yang, E.D. Cranston, S. Zhu, Flexible and porous nanocellulose aerogels with high loadings of metal-organic-framework particles for separations applications, *Adv. Mater.* 28 (2016) 7652–7657, <https://doi.org/10.1002/adma.201601351>.
- [24] R. Guo, X. Cai, H. Liu, Z. Yang, Y. Meng, F. Chen, Y. Li, B. Wang, In situ growth of metal-organic frameworks in three-dimensional aligned lumen arrays of wood for rapid and highly efficient organic pollutant removal, *Environ. Sci. Technol.* 53 (2019) 2705–2712, <https://doi.org/10.1021/acs.est.8b06564>.
- [25] O. Shekhat, J. Liu, R.A. Fischer, Ch. Wöll, MOF thin films: existing and future applications, *Chem. Soc. Rev.* 40 (2011) 1081, <https://doi.org/10.1039/c0cs00147c>.

- [26] H. Li, M. Li, W. Li, Q. Yang, Y. Li, Z. Gu, Y. Song, Three dimensional MOF-sponge for fast dynamic adsorption, *Phys. Chem. Chem. Phys.* 19 (2017) 5746–5752, <https://doi.org/10.1039/C6CP06617H>.
- [27] M.R. Lohe, M. Rose, S. Kaskel, Metal-organic framework (MOF) aerogels with high micro- and macroporosity, *Chem. Commun.* 6056 (2009) <https://doi.org/10.1039/b910175f>.
- [28] D. Zhao, Y. Tian, X. Jing, Y. Lu, G. Zhu, PAF-1@cellulose nanofibril composite aerogel for highly-efficient removal of bisphenol A, *J. Mater. Chem. A* 7 (2019) 157–164, <https://doi.org/10.1039/C8TA09644A>.
- [29] S. Bo, W. Ren, C. Lei, Y. Xie, Y. Cai, S. Wang, J. Gao, Q. Ni, J. Yao, Flexible and porous cellulose aerogels/zeolitic imidazolate framework (ZIF-8) hybrids for adsorption removal of Cr(IV) from water, *J. Solid State Chem.* 262 (2018) 135–141, <https://doi.org/10.1016/j.jssc.2018.02.022>.
- [30] M. Karzar Jehdi, O. Laitinen, H. Liimatainen, Magnetic superabsorbents based on nanocellulose aerobeads for selective removal of oils and organic solvents, *Mater. Des.* 183 (2019) 108115, <https://doi.org/10.1016/j.matdes.2019.108115>.
- [31] D. Matatagui, A. Sainz-Vidal, I. Gràcia, E. Figueras, C. Cané, J.M. Saniger, Chemoresistive gas sensor based on ZIF-8/ZIF-67 nanocrystals, *Sensors Actuators B Chem.* 274 (2018) 601–608, <https://doi.org/10.1016/j.snb.2018.07.137>.
- [32] K.-Y.A. Lin, H.-A. Chang, Ultra-high adsorption capacity of zeolitic imidazole framework-67 (ZIF-67) for removal of malachite green from water, *Chemosphere.* 139 (2015) 624–631, <https://doi.org/10.1016/j.chemosphere.2015.01.041>.
- [33] J.-L. Zhuang, D. Ceglarek, S. Pethuraj, A. Terfort, Rapid room-temperature synthesis of metal-organic framework HKUST-1 crystals in bulk and as oriented and patterned thin films, *Adv. Funct. Mater.* 21 (2011) 1442–1447, <https://doi.org/10.1002/adfm.201002529>.
- [34] G. Majano, J. Pérez-Ramírez, Scalable room-temperature conversion of copper(II) hydroxide into HKUST-1 (Cu₃(btc)₂), *Adv. Mater.* 25 (2013) 1052–1057, <https://doi.org/10.1002/adma.201203664>.
- [35] K. Hyde, H. Dong, J.P. Hinestroza, Effect of surface cationization on the conformational deposition of polyelectrolytes over cotton fibers, *Cellulose.* 14 (2007) 615–623, <https://doi.org/10.1007/s10570-007-9126-z>.
- [36] Z. Xiong, M. Lin, H. Lin, M. Huang, Facile synthesis of cellulose nanofiber nanocomposite as a SERS substrate for detection of thiram in juice, *Carbohydr. Polym.* 189 (2018) 79–86, <https://doi.org/10.1016/j.carbpol.2018.02.014>.
- [37] H. Zhu, B.B. Narakathu, Z. Fang, A. Tausif Ajijazi, M. Joyce, M. Atashbar, L. Hu, A gravure printed antenna on shape-stable transparent nanopaper, *Nanoscale.* 6 (2014) 9110, <https://doi.org/10.1039/C4NR02036G>.
- [38] J. Shao, Z. Wan, H. Liu, H. Zheng, T. Gao, M. Shen, Q. Qu, H. Zheng, Metal organic frameworks-derived Co₃O₄ hollow dodecahedrons with controllable interiors as outstanding anodes for Li storage, *J. Mater. Chem. A* 2 (2014) 12194–12200, <https://doi.org/10.1039/C4TA01966K>.
- [39] H. Liimatainen, J. Sirviö, O. Sundman, O. Hormi, J. Niinimäki, Use of nanoparticulate and soluble anionic celluloses in coagulation-flocculation treatment of kaolin suspension, *Water Res.* 46 (2012) 2159–2166, <https://doi.org/10.1016/j.watres.2012.01.035>.
- [40] J. Guo, I. Filpponen, P. Su, J. Laine, O.J. Rojas, Attachment of gold nanoparticles on cellulose nanofibrils via click reactions and electrostatic interactions, *Cellulose.* 23 (2016) 3065–3075, <https://doi.org/10.1007/s10570-016-1042-7>.
- [41] A. Pei, N. Butchosa, L.A. Berglund, Q. Zhou, Surface quaternized cellulose nanofibrils with high water absorbency and adsorption capacity for anionic dyes, *Soft Matter* 9 (2013) 2047, <https://doi.org/10.1039/c2sm27344f>.
- [42] W. Chen, H. Yu, Q. Li, Y. Liu, J. Li, Ultralight and highly flexible aerogels with long cellulose I nanofibers, *Soft Matter* 7 (2011) 10360, <https://doi.org/10.1039/c1sm06179h>.
- [43] Y. Ji, Y. Wen, Z. Wang, S. Zhang, M. Guo, Eco-friendly fabrication of a cost-effective cellulose nanofiber-based aerogel for multifunctional applications in Cu(II) and organic pollutants removal, *J. Clean. Prod.* 255 (2020) 120276, <https://doi.org/10.1016/j.jclepro.2020.120276>.
- [44] Z. Wang, L. Song, Y. Wang, X.-F. Zhang, D. Hao, Y. Feng, J. Yao, Lightweight UiO-66/cellulose aerogels constructed through self-crosslinking strategy for adsorption applications, *Chem. Eng. J.* 371 (2019) 138–144, <https://doi.org/10.1016/j.cej.2019.04.022>.
- [45] M. Jiao, Y. Yao, C. Chen, B. Jiang, G. Pastel, Z. Lin, Q. Wu, M. Cui, S. He, L. Hu, Highly efficient water treatment via a wood-based and reusable filter, *ACS Mater. Lett.* 2 (2020) 430–437, <https://doi.org/10.1021/acsmaterialslett.9b00488>.
- [46] A.A. Siyal, M.R. Shamsuddin, N.E. Rabat, M. Zulfiqar, Z. Man, A. Low, Fly ash based geopolymer for the adsorption of anionic surfactant from aqueous solution, *J. Clean. Prod.* 229 (2019) 232–243, <https://doi.org/10.1016/j.jclepro.2019.04.384>.
- [47] X. Xu, B. Gao, B. Jin, Q. Yue, Removal of anionic pollutants from liquids by biomass materials: a review, *J. Mol. Liq.* 215 (2016) 565–595, <https://doi.org/10.1016/j.molliq.2015.12.101>.
- [48] J. Shen, X. Wang, L. Zhang, Z. Yang, W. Yang, Z. Tian, J. Chen, T. Tao, Size-selective adsorption of methyl orange using a novel nano-composite by encapsulating HKUST-1 in hyper-crosslinked polystyrene networks, *J. Clean. Prod.* 184 (2018) 949–958, <https://doi.org/10.1016/j.jclepro.2018.03.015>.
- [49] S. Álvarez, R.S. Ribeiro, H.T. Gomes, J.L. Sotelo, J. García, Synthesis of carbon xerogels and their application in adsorption studies of caffeine and diclofenac as emerging contaminants, *Chem. Eng. Res. Des.* 95 (2015) 229–238, <https://doi.org/10.1016/j.cherd.2014.11.001>.
- [50] M. Liu, S. Li, N. Tang, Y. Wang, X. Yang, S. Wang, Highly efficient capture of phosphate from water via cerium-doped metal-organic frameworks, *J. Clean. Prod.* 121782 (2020) <https://doi.org/10.1016/j.jclepro.2020.121782>.
- [51] T. Suopajarvi, J.A. Sirviö, H. Liimatainen, Cationic nanocelluloses in dewatering of municipal activated sludge, *J. Environ. Chem. Eng.* 5 (2017) 86–92, <https://doi.org/10.1016/j.jece.2016.11.021>.
- [52] A.M. Ares, R. Muiño, A. Costoya, R.A. Lorenzo, A. Concheiro, A.M. Carro, C. Alvarez-Lorenzo, Cyclodextrin-functionalized cellulose filter paper for selective capture of diclofenac, *Carbohydr. Polym.* 220 (2019) 43–52, <https://doi.org/10.1016/j.carbpol.2019.05.055>.
- [53] B.N. Bhadra, I. Ahmed, S. Kim, S.H. Jhung, Adsorptive removal of ibuprofen and diclofenac from water using metal-organic framework-derived porous carbon, *Chem. Eng. J.* 314 (2017) 50–58, <https://doi.org/10.1016/j.cej.2016.12.127>.
- [54] S. He, C. Chen, G. Chen, F. Chen, J. Dai, J. Song, F. Jiang, C. Jia, H. Xie, Y. Yao, E. Hitz, G. Chen, R. Mi, M. Jiao, S. Das, L. Hu, High-performance, scalable wood-based filtration device with a reversed-tree design, *Chem. Mater.* 32 (2020) 1887–1895, <https://doi.org/10.1021/acs.chemmater.9b04516>.
- [55] Y. Song, J.Y. Seo, H. Kim, K.-Y. Beak, Structural control of cellulose nanofibrous composite membrane with metal organic framework (ZIF-8) for highly selective removal of cationic dye, *Carbohydr. Polym.* 222 (2019) 115018, <https://doi.org/10.1016/j.carbpol.2019.115018>.
- [56] O. Laitinen, T. Suopajarvi, M. Österberg, H. Liimatainen, Hydrophobic, superabsorbing aerogels from choline chloride-based deep eutectic solvent pretreated and silylated cellulose nanofibrils for selective oil removal, *ACS Appl. Mater. Interfaces* 9 (2017) 25029–25037, <https://doi.org/10.1021/acsami.7b06304>.
- [57] B. Boukoussa, A. Hakiki, S. Moulai, K. Chikh, D.E. Kherroub, L. Bouhadjar, D. Guedal, K. Messaoudi, F. Mokhtar, R. Hamacha, Adsorption behaviors of cationic and anionic dyes from aqueous solution on nanocomposite polypyrrole/SBA-15, *J. Mater. Sci.* 53 (2018) 7372–7386, <https://doi.org/10.1007/s10853-018-2060-7>.